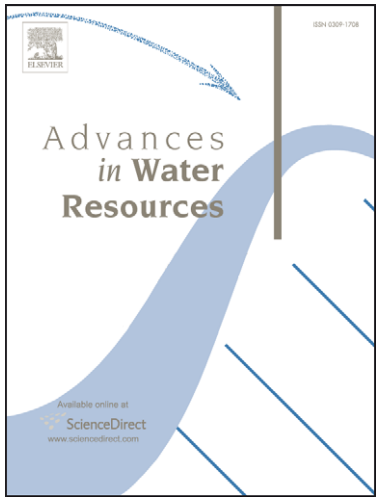

Non-Fickian mixing: temporal evolution of the scalar dissipation rate in porous media

Tanguy Le Borgne, Marco Dentz, Diogo Bolster, Jesus Carrera, Jean-Raynald de Dreuzy, Philippe Davy

PII: S0309-1708(10)00150-8
DOI: 10.1016/j.advwatres.2010.08.006
Reference: ADWR 1593

To appear in: *Advances in Water Resources*

Received Date: 22 March 2010
Revised Date: 11 August 2010
Accepted Date: 12 August 2010

Please cite this article as: Le Borgne, T., Dentz, M., Bolster, D., Carrera, J., de Dreuzy, J-R., Davy, P., Non-Fickian mixing: temporal evolution of the scalar dissipation rate in porous media, *Advances in Water Resources* (2010), doi: 10.1016/j.advwatres.2010.08.006

Non-Fickian mixing: temporal evolution of the scalar dissipation rate in porous media

Tanguy Le Borgne

Geosciences Rennes, UMR 6118, CNRS, Université de Rennes 1, Rennes, France

Marco Dentz

Institute of Environmental Assessment and Water Research (IDÆA-CSIC), Barcelona, Spain

Diogo Bolster

Environmental Fluid Dynamics Laboratories, Dept of Civil Engineering and Geological Sciences, University of Notre Dame, Notre Dame, IN 45665

Jesus Carrera

Institute of Environmental Assessment and Water Research (IDÆA-CSIC), Barcelona, Spain

Jean-Raynald de Dreuzy

Geosciences Rennes, UMR 6118, CNRS, Université de Rennes 1, Rennes, France

Philippe Davy

Geosciences Rennes, UMR 6118, CNRS, Université de Rennes 1, Rennes, France

Abstract

We investigate the temporal scaling properties of mixing in heterogeneous permeability fields with variances ranging from very small ($\sigma^2_{lnK} = 0.01$) to very large ($\sigma^2_{lnK} = 9$). We quantify mixing by the scalar dissipation rate, which we estimate over a large range of temporal scales. For an initial pulse line injection, we find that moderate and strong heterogeneity induce

anomalous temporal scaling of the scalar dissipation rate, which we call non-Fickian mixing. This effect is particularly relevant for upscaling reactive transport as it implies a non-Fickian scaling of reactive transport. Although spreading and mixing are intimately coupled, we find that their scaling properties are not directly related in general. In the Non-Fickian mixing regime, the temporal scaling of the scalar dissipation rate depends on the complex spatial distribution of the concentration field that generates transverse mixing. For times larger than the characteristic diffusion time associated with one permeability field correlation length, the heterogeneity of concentration in the plume is attenuated and progressively erased by diffusion. Thus, at large times, the temporal scaling of mixing and spreading can be related through a simple analytical expression.

1. Introduction

Mixing is a fundamental process that drives chemical reactions in fluids (Rezaei et al., 2005; Cirpka and Valocchi, 2007; Tartakovsky et al., 2008a; de Simoni et al., 2005, 2007). Understanding and predicting mixing is a key step for predicting reactive transport as it describes the rate at which reactants will meet. Therefore, it has attracted the attention of researchers across a range of scientific communities. In geophysical flows, mixing finds applications both in porous media flow (Kitanidis, 1994; Kapoor and Kitani-

dis, 1998; Kleinfelter et al., 2005) and in turbulent flows at various scales as found in oceanic and atmospheric flows (Pope, 2000; Weiss and Provenzale, 2008; Rees, 2006). Heterogeneous velocity fields, which fluctuate at multiple scales, are typical in these applications. The flow heterogeneity generates complex concentration distributions that enhance mixing (e.g., Pope, 2000; Tartakovsky et al., 2008b).

For transport in heterogeneous porous media, a fundamental difference exists between the concepts of spreading and mixing (Kitanidis, 1988, 1994). Spreading describes the spatial extent of a solute plume, while mixing can be seen as the process that increases the actual volume occupied by the solute. Thus, the processes of spreading and mixing may be quantified in terms of (suitably defined) moments of the concentration distribution (e.g., Kitanidis, 1988; Attinger et al., 1999; Dentz et al., 2000; Dentz and Carrera, 2007; Dentz et al., 2010). Mixing can also be seen as the process that smoothes out concentration contrasts, or in other words homogenizes a given (heterogeneous) concentration distribution. Various measures for quantifyng mixing have been proposed. For example, the dilution index is a mixing measure based on entropy concepts (Kitanidis, 1994) that quantifies the volume occupied by the solute. As such it measures the mixing state of a plume. On the other hand, the mean scalar dissipation rate, defined from the local concentration gradients quantifies the mixing rate (e.g., Pope, 2000). The mixing

state and mixing rate evolve with time in opposite directions.

Spreading and mixing are stronlgy coupled (e.g., Kitanidis, 1988, 1994). Spreading is essentially driven by advective mechanims and tends to enhance concentration contrasts, which in turn enhance mixing. Various studies on effective mixing and reactive transport for moderately heterogeneous media exist (Kapoor and Gelhar, 1994a,b; Kapoor and Kitanidis, 1998; Fiori and Dagan, 2002; Luo et al., 2008; Cirpka et al., 2008; Fernandez-Garcia et al., 2008). These are typically based on perturbation methods and restricted to moderately varying permeability fields. Mixing has not been analyzed for highly heterogeneous permeability fields. The high degree of heterogeneity implies that the large scale spreading of a solute plume is non-Fickian over a large range of times (Matheron and de Marsily, 1980; Fiori et al., 2006; Berkowitz et al., 2006; Benson et al., 2001; Cushman et al., 2005; Le Borgne and Gouze, 2007; Le Borgne et al., 2008a; Neuman and Tartakovsky, 2009; Zhang et al., 2009). Non-Fickian spreading can be characterized by the scaling of the characteristic plume size, σ_1, defined as the standard deviation of the spatial distribution of concentrations:

$$\sigma_1^2(t) = \frac{1}{L_x} \int_\Omega \mathrm{d}^d x \left[x_1 - \langle x_1(t) \rangle\right]^2 c(\mathbf{x}, t). \tag{1}$$

where $\langle x_1(t) \rangle$ is the center of mass coordinate of the plume in the direction of mean flow, which here is aligned with the one-direction of the coordinate system. The broad interest in non-Fickian spreading constrats with the

paucity of similar work on mixing. The objective of our work is precisely to investigate the relationship between non-Fickian spreading and non-Fickian mixing.

We start by introducing the mixing measure that we consider, the scalar dissipation rate and show that it is related to effective reaction laws. We propose an efficient numerical method to quantify the temporal scaling of the scalar dissipation with high accuracy. Using this method, we quantifiy the temporal scaling of spreading and mixing. We demonstrate the occurence of non-Fickian mixing, even for cases that appear to be Fickian from a spreading perspective, and discuss its physical origin.

2. The Scalar dissipation rate

We consider transport by diffusion and advection in a heterogeneous velocity field. We quantify global mixing by the scalar dissipation rate (e.g., Pope, 2000; Kapoor and Anmala, 1998; Kapoor and Kitanidis, 1998; Fedotov et al., 2005; Warhaft, 2000; Bolster et al., 2010b), which is a global measure of mixing defined as

$$\chi(t) = \int_{\Omega} \mathrm{d}^d x D \nabla c(\mathbf{x}, t) \cdot \nabla c(\mathbf{x}, t), \tag{2}$$

where D is the constant diffusion coefficient, c is the local concentration and d is the Eulerian dimension of space. Note that for simplification we do not

consider a local dispersion tensor in this study. The methods and analysis presented can however readily be extended to take this into account.

The interest of the scalar dissipation rate as a mixing measure can be understood from the work of de Simoni et al. (2005, 2007), which we briefly summarise here. Consider the transport of two reacting species of concentrations $c_1(x,t)$ and $c_2(x,t)$, which react in equilibrium to produce a third immobile component $c_3(x,t)$. The governing equations can be written as

$$\frac{\partial c_i}{\partial t} + \mathbf{v}(\mathbf{x}) \cdot \nabla c_i = D\nabla^2 c_i + r(\mathbf{x},t), i = 1,2 \tag{3}$$

and

$$\frac{\partial c_3}{\partial t} = -r(\mathbf{x},t), \qquad c_1 c_2 = K_c, \tag{4}$$

where $\mathbf{v}(\mathbf{x},\mathbf{t})$ is the velocity field, D is the diffusion coefficient, assumed to be identical for all components, $r(\mathbf{x},t)$ is the equilibrium reaction rate and K_c is the chemical equilibrium constant. A conservative component for this reactive transport system can be defined as $c(\mathbf{x},t) = c_1(\mathbf{x},t) - c_2(\mathbf{x},t)$. Substracting the transport equations (3) for c_1 and c_2, it can be shown that c satisfies the pure advection diffusion equation, which is the same as (3) but with $r = 0$. This shows that c is indeed conservative.

Using (4) and the definition of c allows us to solve for $c_1(c)$ and $c_2(c)$. Substituting the latter in (4), while using the fact that c is conservative yields

$$r_2(\mathbf{x},t) = \left(\frac{d^2 c_2}{dc^2}\right) D\nabla c \cdot \nabla c, \tag{5}$$

where the first term d^2c_2/dc^2 is called the chemical factor and depends on the specifics of the reaction (stoichiometry and equilibrium constant). The second term $D\nabla c \cdot \nabla c$, called the mixing factor, is exactly the integrand of the scalar dissipation rate defined in (2). From (5) we can define the global reaction rate as:

$$R_2(t) = \int_\Omega \mathrm{d}^d x \frac{\mathrm{d}^2 c_2}{\mathrm{d}c^2} D\nabla c \cdot \nabla c \tag{6}$$

When the chemical factor varies little over the range of $c(\mathbf{x}, t)$ considered (Fernandez-Garcia et al., 2008; Sanchez-Vila et al., 2008), it can be assumed to be almost constant and thus the global reaction rate is directly proportional to the scalar dissipation rate. Note however that when the chemical factor varies strongly with the mixing ratio such a global measure is not sufficient for predicting reactions (Willmann et al., 2010; Bolster et al., 2010a). In general, if the scalar dissipation rate temporal scaling is anomalous, i.e. the mixing process is non-Fickian, the reaction rate temporal scaling is also expected to be anomalous. Thus, understanding the scaling behaviour of the scalar dissipation rate is an important first step for upscaling reactive transport.

One of the main difficulties in evaluating the scalar dissipation rate and reactions for that matter is the numerical calculation of the concentration gradients in equations (2) and (6). The concentration field can vary sharply over small distances, particularly for highly heterogeneous velocity fields.

An accurate quantification of concentration gradients requires a very fine discretization for Eulerian numerical schemes, where numerical dispersion can induce errors, or a very large number of particles for random walk approaches. Concentration gradients are very sensitive to numerical noise in the concentration field. To circumvent this issue, Fernandez-Garcia et al. (2008) proposed an interpolation procedure to obtain a smooth concentration field from a limited number of particles. While appealing and useful in practice, such interpolation methods must be conducted with caution as they can lead to smoothing of actual gradients. A lack of resolution of these gradients can seriously compromise the ability of any model to accurately predict mixing and reactions (Battiato et al., 2009).

Global mixing measures such as the scalar dissipation rate, can be determined without the computation of the local concentration gradients. Instead one can evaluate the scalar dissipation rate from the integral of the squared concentration (e.g., Pope, 2000), defined as

$$M(t) = \int_{\Omega} \mathrm{d}^d x c^2. \tag{7}$$

For advective-diffusive transport in a domain with no solute flux boundary conditions, the scalar dissipation rates can be expressed as

$$\chi(t) = -\frac{1}{2}\frac{\mathrm{d}M}{\mathrm{d}t}. \tag{8}$$

The equivalence of expressions (8) and (2) can be seen by multiplying the

advection-dispersion equation in (4) for $r(\mathbf{x}, t) = 0$ by c and integrating over space, using the divergence theorem. This is detailed in appendix A Notice that $M(t)$ should not be confused with spatial or temporal moments of concentration. It quantifies the variability of the concentration values at a given time and not the temporal or spatial extent of the plume.

We now illustrate that calculating the scalar dissipation rate using $M(t)$ is significantly better than calculating it from local gradients of concentration. We solve the advection-diffusion equation for a homogeneous medium and an initial line injection using a particle tracking method. We take a permeameter geometry with homogeneous velocity v and diffusion coefficient D. Snapshots of the calculated concentration distributions are shown in Fig. 1. The time is normalized by the characteristic diffusion time over one pixel $\tau_D = \Delta x^2/D = 3$, where Δx is the pixel size. The local concentration is normalized by the total mass so that $\int_\Omega \mathrm{d}^d x c(\mathbf{x}) = 1$. For such system, the analytical solution for the scalar dissipation rate is obtained by replacing the ADE solution in $2D$ in equation (2), which yields,

$$\chi_{1D}(t) = \frac{C_0^2 L_y t^{-3/2}}{8\sqrt{2\pi D}}, \tag{9}$$

where C_0 is the initial concentration and L_y is the size of the domain in the vertical direction.

Figure 1:

Although we used a relatively large number of particles ($N = 10^5$), the concentration field is poorly resolved at late time due to the dilution of the plume. Even at the earliest time in Fig. 1 it is clear that the numerical field does not vary as smoothly as the analytical solution. The noise in the concentration field makes it next to impossible to accurately evaluate the scalar dissipation by gradients as it induces non physical gradients. This is clearly seen in Fig. 2 where the gradient method in equation (6) significantly overestimates the scalar dissipation rate after a relatively short time. Conversely, despite poor resolution of the concentration field, the scalar dissipation rate estimated from the temporal derivative of $M(t)$ in (8) is in very close agreement with the analytical solution over the full range of time and concentration scales considered (Fig. 2).

The error on the estimation of the scalar dissipation rate depends on the bin size for computing concentrations and on the number of particles. For a too large bin size, the averaging of the concentration field implies that its variability is under-estimated. Here, we take a bin size equal to the velocity field discretization. In Appendix A, we show that, for a given bin size, the relative mean error of the scalar dissipation rate due to a finite number N of particles is given by

$$\frac{\Delta\chi_N(t)}{\chi(t)} = \frac{1}{2N}. \tag{10}$$

Further analysis of the effect of a finite number of particles on the concentra-

tion statistics can be found in Feller (1971) and Chakraborty et al. (2009). In summary, we deem the temporal derivative of $M(t)$ to be a robust estimator of the actual scalar dissipation rate $\chi(t)$.

3. Non-Fickian mixing

We now consider transport in a two-dimensional multi-lognormal hydraulic conductivity field defined by its log-conductivity variance σ^2_{lnK} and a Gaussian correlation with correlation length λ. In order to compare the scalings of spreading and mixing, we study the temporal behavior of the spreading length $\sigma_1(t)$ and scalar dissipation rate $\chi(t)$ for different permeability field variances σ^2_{lnK}. Note that the scaling behavior will also depend in general on the permeability field representation (multi-lognormal, connected or stratified), the permeability field correlation length and the injection mode. However, our aim here is not to perform an exhaustive analysis for all these different conditions. We study spreading and mixing for a single realization, with large dimension so that we can analyze scaling behavior over 3 orders of magnitude in time. For the domain sizes investigated the results depend only slightly on the particular realization. Note that the methodology can be easily extended to $3D$. However, obtaining a large range of simulation times in $3D$ domains currently typically requires using parallel simulations (de Dreuzy et al., 2007).

We adopt a domain of size $\Omega = [0, L_1] \times [0, L_2]$, where L_1 is the size in the direction parallel to the mean flow direction and L_2 is the size perpendicular to the mean flow direction. The boundary conditions are again permeameter-like. The steady flow is divergence-free, $\nabla \cdot \mathbf{q}(\mathbf{x}) = 0$. It is obtained from the Darcy equation $\mathbf{q}(\mathbf{x}) = -K(\mathbf{x})\nabla h(\mathbf{x})$, together with prescribed head conditions on the vertical boundaries and no-flow conditions across the horizontal boundaries; $K(\mathbf{x})$ is the hydraulic conductivity and $h(\mathbf{x})$ is the hydraulic head.

Transport is solved by a random walk particle tracking scheme (Kinzelbach, 1988; Salamon et al., 2006), which prevents numerical dispersion problems for highly heterogeneous media. We define the Peclet number as $Pe = \lambda K_g \nabla h / \Phi D = \lambda \overline{v} / D$, where K_g is the geometric mean of the hydraulic conductivity, ∇h is the mean hydraulic gradient Φ is the constant porosity, and $\overline{v}$ is the mean velocity. The domain size is $8192 \times 1024 = 819.2\lambda \times 102.4\lambda$.

We study the mixing behavior for an initial instantaneous line injection. Results are sensitive to the way the injection is performed. Therefore, this issue deserves some discussion. The most immediate option is to adopt a constant injection by setting an equal number of particles in each pixel of the line. The issue with this injection method is that the probability of injecting particles into very low velocity zones is larger than that of particles entering low velocity zones while travelling through the medium. The con-

sequence is that islands of high concentration zones are created in very low velocity regions, from which particles can only leave by diffusion. This effect dominates the mixing behavior and thus introduces a bias in the analysis.

The above problem suggests that the most realistic option is the flux proportional injection, where the number of particles injected in each region is proportional to the local flux. The advantage of this method is that the initial probability distribution of particle velocities is the same as the Lagrangian velocity distribution. However, this injection method implies a large initial variance of concentration since the local concentration is proportional to the number of particles. This initial variance reflects the fact that more initial mass enters into the high flow regions, which may be considered natural, but hinders comparisons of mixing for different permeability fields, because the initial concentration (i.e. the mixing state) depends on the permeability field variance. To overcome this problem, we also adopted a hydrib injection method, which we term fully mixed constant injection. It consists of injecting the particles with a constant injection (i.e. equal number of particles in each pixel). But, to avoid trapping of particles in low velocity regions, we impose a fully mixed condition at the injection line by setting a large transverse diffusion coefficient in the first pixel. The advantage of this method is that the initial concentration variance is independent on the permeability field heterogeneity while at the same time the number of particles injected

effectively in each flow zone of the second pixel row is proportional to the local flux. Obviously the problem with this injection condition is that a large amount of mixing occurs in the injection row of pixels. Fig. 4b compares the scalar dissipation rate estimated with the latter injection condition to that estimated from the flux proportional injection. For the weakly heterogeneous field, the two injection methods give the same result. For the intermediate and strong heterogeneity cases, the scalar dissipation rate estimated from the flux proportional method is larger at early time than that obtained from the fully mixed constant injection method. This is due to the larger initial concentration variance for the flux proportional injection method. However, at intermediate and large times, the two injection methods give the same results. This indicates that the memory of the initial injection condition on mixing is relatively short (on the order of $3\tau_a$). In the following, we discuss the results for the fully mixed constant injection method.

Examples of simulated concentration fields at different travel times are given in Fig. 3, for a permeability field variance $\sigma^2_{\ln K} = 9$, correlation length $\lambda = 10\Delta x$ and Peclet number $Pe = 10^2$. The temporal evolution of the characteristic plume size for different permeability field variances is shown in Fig. 4a. The time is normalized by the characteristic advection time $\tau_a = \lambda/\overline{v}$, where $\overline{v}$ is the mean velocity. The spreading length is normalized by the permeability field correlation length λ. The temporal evolution of the

characteristic plume size for a small permeability field variance of $\sigma^2_{\ln K} = 0.01$ is Fickian over most of the temporal range, i.e. $\sigma_1 \propto t^{1/2}$. For an intermediate permeability field variance $\sigma^2_{\ln K} = 1$, the evolution of σ_1 is intially non-Fickian, but returns to the Fickian scaling, for $t > 10\tau_a$. One needs to bear in mind the large size of the initial plume to understand how quickly the Fickian regime is attained. However, for the largest permeability field variance, the evolution of σ_1 is non-Fickian over the full temporal range investigated here. Note that we also computed the characteristic plume size averaged over 100 realizations (Le Borgne et al., 2008a,b). The results are less noisy but the non-Fickian scaling obtained is the same.

The temporal evolution of the scalar dissipation rate is shown in Fig. 4b for different variances of the permeability field. $\chi(t)$ is normalized by $\chi_{1D}(\tau_a)$ (9). At early times ($t < 3\tau_a$), the scalar dissipation rate scaling is independent on the permeability field heterogeneity and follows the Fickian scaling, which reflects the large mixing at the initial condition (in the flux-averaged initial condition, the mixing rate is higher for large variances, which reflects that the initial state is less mixed). For both the intermediate ($\sigma^2_{\ln K} = 1$) and large heterogeneities ($\sigma^2_{\ln K} = 9$) cases the scaling of the scalar dissipation rate is found to be non-Fickian at larger times. Such non-Fickian scaling occurs despite the late time Fickian behaviour in longitudinal spreading for the intermediate heterogeneity case. Thus, mixing can be said to be more

"anomalous" than spreading. A similar result was obtained by Vanderborght et al. (2006) that showed that mixing may be non-Fickian also for cases that appear to be Fickian from a spreading perspective.

In the non-Fickian regime, the slope of the scalar dissipation rate evolution with time reflects the dimensionality of the mixing process. Non-Fickian mixing occurs due to transverse diffusion when new interfaces are created by shearing of the plume (Werth et al., 2006). The heterogeneous velocity fields induce plume stretching and concentration gradients in all directions and not only in the longitudinal direction as for the homogeneous case. For a $2D$ mixing process, as occurs for a point injection in a homogeneous media, the scalar dissipation rate scales as $\chi(t) \propto t^{-5/2}$. Here we find a scaling that is intermediate between the $1D$ and $2D$ behaviours. The transition time between the Fickian and non-Fickian mixing regimes decreases with the permeability heterogeneity. For the intermediate heterogeneity it is approximately equal to $10\tau_a$ while for the strong heterogeneity case it is approximately equal to $3\tau_a$. This is the time necessary for spreading to create new interfaces aligned with the direction of flow.

The cumulative scalar dissipation, $\int_0^t \mathrm{d}t\chi(t) = 1/2(M(0) - M(t))$, represents the total amount of mixing that has occured up untill time t. The temporal evolution of $M(t)$ is shown in Fig.5. It is normalized by its expected value for the homogenenous domain at time $t = \tau_a$, $M_{1D}(\tau_a)$. $M(t)$ is

initially independent on the permeability field variance and decreases faster for the largest heterogeneity. Thus, the total cumulative mixing at a given time increases witht the permeability field heterogeneity.

4. Effect of the plume spatial structure and transverse concentration gradients

The non-Fickian scaling of mixing is partly due to incomplete mixing inside the plume, which generates concentration gradients in the transverse direction, and partly due to non-Fickian spreading, which influences the concentration gradients in the longitudinal direction. To analyze these two effects, we define the longitudinal scalar dissipation rate, which quantifies the longitudinal mixing rate, and compare it to the scalar dissipation rate estimated from the full concentration field. A similar analysis was conducted analytically for a confined stratified medium by Bolster et al. (2010b). For this, we define the mean longitudinal concentration projected in the transverse direction $\overline{c}(x_1, t)$ as

$$\overline{c}(x_1, t) \equiv \prod_{i \neq 1} \frac{1}{L_i} \int_0^{L_i} dx_i c. \tag{11}$$

The integral of the squared projected concentration is

$$M_1(t) = \int_0^{L_1} dx_1 \overline{c}^2 \tag{12}$$

and thus the longitudinal scalar dissipation rate is

$$\chi_1(t) = -\frac{1}{2}\frac{\mathrm{d}M_1}{\mathrm{d}t} = \int_0^{L_1} D\left(\frac{\partial \overline{c}}{\partial x_1}\right)^2. \tag{13}$$

The longitudinal scalar dissipation rate represents the contribution of the longitudinal concentration gradients to the global dissipation rate. For weakly heterogeneous permeability fields, the scalar dissipation rate estimated from the projected concentration field is very close to that estimated from the full concentration field (Fig. 6a), reflecting the fact that the projected concentration field is a relatively good measure of the actual one. This is expected since the induced transverse concentration gradients are very small for this case. This result also demonstrates the robustness of our method for estimating the scalar dissipation rate. The full concentration field is much noisier than the projected concentration field, due to a lower density of particles, as illustrated in Fig. 1. Nonetheless, the scalar dissipation rates estimated from the two concentration fields are very similar. For the intermediate and strong heterogeneity cases, $\chi(t)$ and $\chi_1(t)$ diverge significantly (Fig. 6b and c). This quantifies the preponderant role that transverse concentration gradients within the plume play on mixing.

For the intermediate heterogeneity field, the temporal evolution of the longitudinal scalar dissipation rate is initially non-Fickian and then converges to Fickian (Fig. 6b) for $t/\tau_a = 10$, which is the time for which spreading

becomes Fickian (Fig. 4a). For the strong heterogeneity field, the temporal evolution of the longitudinal scalar dissipation rate is non-Fickian at all times (Fig. 6c). Thus, the non-Fickian behavior of longitudinal mixing appears to occur for the same time ranges as the non-Fickian behavior of spreading. This observation leads us to conjecture that the relationship between longitudinal mixing and spreading might be the same as for the Fickian case. For the homogeneous case, the relationship between $\chi_1(t)$ and $\sigma_1(t)$ is given by

$$\chi_1(t) = \frac{1}{4\sqrt{\pi}\sigma_1^2}\frac{\mathrm{d}\sigma_1}{\mathrm{d}t}. \tag{14}$$

In Fig. 6 we illustrate that relationship (14) appears to correctly predict this relationship not only for the weak heterogeneity case, but also for the intermediate and strong heterogeneity cases. This suggests that equation (14) is generally valid for Fickian and non-Fickian transport and that it can quantify the impact of anomalous spreading on longitudinal mixing. This can be shown to be true for non-Fickian transport governed by the fractional ADE (Bolster et al., 2010a). Note that for the strong heterogeneity case, equation (14) is only verified for $t > 10\tau_a$.

For most of the temporal range, the scaling of $\chi(t)$ is different from that of $\chi_1(t)$. This implies that transerve concentration gradients have a preponderant role in governing the scaling non-Fickian scaling of $\chi(t)$. For this reason, transport models calibrated from global spreading measures generally cannot be used directly for predicting mixing and reactive transport (Cirpka and Ki-

tanidis, 2000a,b). However, at late times, concentration gradients have been significantly erased by diffusion and the concentration field appears to be more homogeneous (Fig. 3d). A characteristic time for this process is the time for Lagrangian particles to diffuse across one correlation length of the heterogeneity $\tau_D = \frac{\lambda^2}{D}$. This is the time needed for diffusion to fill the holes in the concentration field, that are created by the presence of low velocity regions. For $t > \tau_D$, the scalar dissipation rate $\chi(t)$ appears to converge towards $\chi_1(t)$. The effect of the plume structure on the scalar dissipation rate becomes negligible compared to the effect of the global spreading of the plume. This implies that, after this time, an effective transport model based on longitudinal spreading can correctly represent mixing processes, which may explain the results of Willmann et al. (2010). It is important to emphasize, however, that at time later than τ_D the spreading rate, can and will continue to be non-Fickian. In this regime, mixing can be therefore be predicted by equation (14).

5. Conclusion

We demonstrate the occurence of a non-Fickian scaling of mixing in heterogeneous porous media. This effect is due to ramified patterns of the dispersion front that imply that diffusive mass transfer occurs in all directions and across numerous interfaces within the plume and not only in the direc-

tion parallel to the mean flow or at the plume edge. Thus, the non-Fickian scaling of mixing reflects the *dimensionality* of the mixing process. Although mixing and spreading are intimately related processes, there is no direct relationship between their temporal scalings. Mixing can be non-Fickian when spreading is Fickian and vice versa. Only when internal concentration gradients have been erased by diffusion within the plume can the two processes be related by a simple analytical relationship. This occurs after the diffusion time τ_D that characterizes the time for diffusion across the permeability field correlation lenght.

The scalar dissipation rate is of particular interest as a measure of mixing as it is directly tied to the temporal evolution of reaction rates. From the results obtained here we can anticipate an anomalous scaling of reaction rates in highly heterogeneous media. This will have important consequences for upscaling reactive transport in heterogeneous porous media. The methodology presented here, which consists of evaluating the scalar dissipation as the time derivative of the integral of the squared concentration, is particularly efficient to investigate such effect as it circumvents having to compute local concentration gradients. As such, it allows an accurate estimation of the scalar dissipation rate over many orders of magnitude in time. The methodology will be extended to $3D$ and used to investigate the influence of the injection mode, the permeability field representation and correlation

structure.

Figure 2:

Figure 3:

Figure 4:

6. Ackowledgments

We acknowledge the financial help of the French National Research Agency, through the projects MOHINI (ANR-07-VULN-008) and MICAS (ANR-07-CIS7-004). The financial support of the European Commission through FP7 projects MUSTANG and CIUDEN and ITN project IMVUL (grant agreement 212298) is gratefully acknowledged. Tanguy Le Borgne acknowlegdes the support of the Marie Curie ERG grant ReactiveFlows (Grant Agreement Number 230947).

7. Bibliography

References

Attinger, S., Dentz, M., Kinzelbach, H., Kinzelbach, W., 1999. Temporal behavior of a solute cloud in a chemically heterogenous porous medium,. J. Fluid Mech. 386, 77–104.

Figure 5:

Figure 6:

Battiato, I., Tartakovsky, A., Tartakovsky, D., Scheibe, T., 2009. On breakdown of macroscopic models of reactive transport in porous media. Advances in Water Resources 32, 1664–1673 doi:10.1016/j.advwatres.2009.08.008.

Benson, D., Schumer, R., Meerschaert, M., Wheatcraft, S., 2001. Fractional dispersion, lvy motion, and the made tracer tests. Transport in Porous Media 42, 211–240.

Berkowitz, B., Cortis, A., Dentz, M., Scher, H., 2006. Modeling non-Fickian transport in geological formations as a continuous time random walk. Rev. Geophys. 44, 2005RG000178.

Bolster, D., Benson, D., Le Borgne, T., Dent, M., 2010a. Anomalous mixing and reaction induced by super-diffusive non-local transport. Phys. Rev. E in press.

Bolster, D., Valdes-Parada, F. J., Le Borgne, T., Dentz, M., Carrera, J., 2010b. Mixing in confined stratified aquifers. J. of Cont. Hydrol., doi: 10.1016/j.jconhyd.2010.02.003.

Chakraborty, P., Meerschaert, M., Lim, C. Y., 2009. Parameter estimation

for fractional transport: A particle tracking approach. Water Resour. Res. 45, W10415, doi:10.1029/2008WR007577.

Cirpka, O., Kitanidis, P., 2000a. An advective-dispersive streamtube approach for the transfer of conservative tracer data to reactive transport. Water Resour. Res. 36, 1209–1220.

Cirpka, O., Kitanidis, P., 2000b. Characterization of mixing and dilution in heterogeneous aquifers by means of local temporal moments. Water Resour. Res. 36, 1221–1236.

Cirpka, O. A., Schwede, R. L., Luo, J., M., D., 2008. Concentration statistics for mixing-controlled reactive transport in random heterogeneous media. J. of Cont. Hydrol. 98, 61–74.

Cirpka, O. A., Valocchi, A. J., 2007. Two-dimenstional concentration distribution for mixing-controlled bioreactive transport in steady-state. Adv. in Water Resour. 30, 1668–1679.

Cushman, J. H., Park, M., Kleinfelter, N., Moroni, M., 2005. Super-diffusion via levy lagrangian velocity processes. Geophysical Research Letters 32, L19816.

de Dreuzy, J.-R., Beaudoin, A., Erhel, J., 2007. Asymptotic dispersion in 2d

heterogeneous porous media determined by parallel numerical simulations. Water Resour. Res. 43, W10439.

de Simoni, M., Carrera, J., Sanchez-Vila, X., Guadagnini, A., 2005. A procedure for the solution of multicomponent reactive transport problems. Water Resources Research 10.1029/2005WR004056, W11410.

de Simoni, M., Sanchez-Vila, X., Carrera, J., Saaltink, M., 2007. A mixing ratios-based formulation for multicomponent reactive transport. Water Resour. Res. 43, W07419.

Dentz, M., Carrera, J., 2007. Mixing and spreading in stratified flow. Phys. Fluids 19, 017107.

Dentz, M., Kinzelbach, H., Attinger, S., Kinzelbach, W., 2000. Temporal behavior of a solute cloud in a heterogeneous porous medium, 1, point-like injection. Water Resour. Res. 36 (12), 3591–3604.

Dentz, M., Le Borgne, T., Englert, A., Bijeljic, B., 2010. Mixing, spreading and reaction in heterogeneous media: A brief review. J. Contam. Hydrol. doi:10.1016/j.jconhyd.2010.05.002.

Fedotov, S., Ihme, M., Pitsch, H., 2005. Stochastic mixing model with power law decay of variance. Phys. Rev. E 71 (1), 016310.

Feller, W., 1971. An introduction to probability theory and its applications. Wiley.

Fernandez-Garcia, D., Sanchez-Vila, X., Guadagnini, A., 2008. Reaction rates and effective parameters in stratified aquifers. Adv. in Water Resour. 31, 1364–1376.

Fiori, A., Dagan, G., 2002. Transport of a passive scalar in a stratified porous medium. Transport in Porous Media 47, 81–98.

Fiori, A., Jankovic, I., Dagan, G., 2006. Modeling flow and transport in highly heterogeneous three-dimensional aquifers: Ergodicity, gaussianity, and anomalous behavior- 2. approximate semianalytical solution. Water Resour. Res. 42, W06D13.

Kapoor, V., Anmala, J., 1998. Lower bounds on scalar dissipation in bounded reactilinear flows. Flow, turbulence and combustion 60, 125–156.

Kapoor, V., Gelhar, L. W., 1994a. transport in three-dimensionally heterogeneous aquifers: 1. dynamics of concentration fluctuations. Water Resour. Res. 30, 1775–1788.

Kapoor, V., Gelhar, L. W., 1994b. transport in three-dimensionally heterogeneous aquifers: 2. predictions and observations of concentration fluctuations. Water Resour. Res. 30.

Kapoor, V., Kitanidis, P. K., 1998. Concentration fluctuations and dilution in aquifers. Water Resour. Res. 34, 1181–1193.

Kinzelbach, W., 1988. The random-walk method in pollutant transport simulation. In: NATO ASI Ser. No. 224. pp. 227–246.

Kitanidis, P. K., 1988. Prediction by the method of moments of transport in heterogeneous formations. J. Hydrol. 102, 453–473.

Kitanidis, P. K., 1994. The concept of the dilution index. Water Resour. Res. 30, 20112026.

Kleinfelter, N., Moroni, M., Cushman, J. H., 2005. Application of the finite-size lyapunov exponent to particle tracking velocimetry in fluid mechanics experiments. Phys. Rev. E 72 (5), 056306.

Le Borgne, T., Dentz, M., Carrera, J., 2008a. Lagrangian statistical model for transport in highly heterogeneous velocity fields. Phys. Rev. Lett. 101 (9), 090601.

Le Borgne, T., Dentz, M., Carrera, J., 2008b. Spatial markov processes for modeling lagrangian particle dynamics in heterogeneous porous media. Phys. Rev. E 78 (2), 026308.

Le Borgne, T., Gouze, P., 2007. Non-fickian dispersion in porous media: 2.

model validation from measurements at different scales. Water Resour. Res. 44, W06427.

Luo, J., Dentz, M., Carrera, J., P., K., 2008. Effective reaction parameters for mixing controlled reactions in heterogeneous media. Water Resour. Res. 44, W02416.

Matheron, G., de Marsily, G., 1980. Is transport in porous media always diffusive? a counterexample. Water Resources Res 16, 901.

Neuman, S. P., Tartakovsky, D. M., 2009. Perspective on theories of anomalous transport in heterogeneous media. Adv. Water Resour. 32, doi:10.1016/j.advwatres.2008.08.005.

Pope, S. B., 2000. Tubulent Flows. Cambridge University Press.

Rees, J., 2006. Mixing in geophysical and astrophysical flows. Environmental Fluid Mechanics 1, 333–343.

Rezaei, M., Sanz, E., Raeisi, E., Ayora, C., Vzquez-Su, E., Carrera, J., 2005. Reactive transport modeling of calcite dissolution in the fresh-salt water mixing zone. Journal of Hydrology 311, 282298.

Salamon, P., Fernandez-Garcia, D., Gomez, J., 2006. A review and numerical assesment of the random walk particle tracking method. Journal of Contaminant Hydrology 87, 277–305.

Sanchez-Vila, X., Fernandez-Garcia, D., Guadagnini, A., 2008. Conditional probability density functions of concentrations for mixing-controlled reactive transport in heterogeneous aquifers. Mathematical Geosciences 41, 323–351.

Tartakovsky, A. M., Redden, G., Lichtner, P. C., Scheibe, T. D., Meakin, P., 2008a. Mixing-induced precipitation: Experimental study and multiscale numerical analysis. Water Resour. Res. 44, W06S04.

Tartakovsky, A. M., Tartakovsky, D. M., Meakin, P., 2008b. Stochastic langevin model for flow and transport in porous media. Phys. Rev. Lett. 101 (4), 044502.

Vanderborght, J., Kasteel, R., Vereecken, H., 2006. Stochastic continuum transport equations for field-scale solute transport: Overview of theoretical and experimental results. Vadose Zone J. 5, 529–538.

Warhaft, Z., 2000. Passive scalars in turbulent flows. Ann. Rev. Fluid Mech 32 (1), 203–240.

Weiss, J., Provenzale, A., 2008. Transport and mixing in geophysical flows. Springer, Berlin.

Werth, C. J., Cirpka, O. A., Grathwohl, P., 2006. Enhanced mixing and reac-

tion through flow focusing in heterogeneous porous media. Water Resour. Res. 42, W12414.

Willmann, M., Carrera, J., Snchez-Vila, X., Silva, O., Dentz, M., 2010. Coupling of mass transfer and reactive transport for non-linear reactions in heterogeneous media. Water Resour. Res. W07512, doi:10.1029/2009WR007739.

Zhang, Y., Benson, D., Reeves, D., 2009. Time and space nonlocalities underlying fractional-derivative models: Distinction and literature review of field applications. Advances in Water Resources 32, 561–581.

8. Figure captions

Figure 1. (color online). Spatial distribution of the concentration $c(x,t)$ simulated with 10^5 particles in a homogeneous porous medium at times a) $t/\tau_D = 12.2$, b) $t/\tau_D = 127.6$, c) $t/\tau_D = 321$. The color scale shows the logarithm of the concentration, computed with a bin size equal to the pixel size Δ_x.

Figure 2. Time evolution of the scalar dissipation rate in a homogeneous medium, estimated from local concentration gradients and from the time derivative of $M(t)$. Notice the perfect overlap of the latter with the analytical solution.

Figure 3. (color online). Spatial distribution of the conservative component $c(x,t)$ simulated for 10^6 particles in a highly heterogeneous porous medium at times a) $t/\tau_a = 0.8$, b) $t/\tau_a = 2.6$, c) $t/\tau_a = 8.2$, d) $t/\tau_a = 82$. The color scale shows the logarithm of the concentration, computed with a bin size equal to the pixel size Δ_x. The permeability field variance is $\sigma^2_{\ln K} = 9$, the correlation length $\lambda = 10$ and the Peclet number $Pe = 10^2$.

Figure 4. a) Characteristic spreading length (longitudinal standard deviation of the plume) and b) scalar dissipation rate estimated for permeability field variances ranging from $\sigma^2_{\ln K} = 0.01$ to $\sigma^2_{\ln K} = 9$ for a Peclet number $Pe = 10^2$.

Figure 5. Time evolution of $M(t)$ for different permeability field variances. $M(t)$ is normalized by its expected value for the homogenenous domain at time $t = \tau_a$, $M_{1D}(\tau_a)$.

Figure 6. Scalar dissipation rate estimated from the full concentration field $\chi(t)$ (full line), compared to that estimated from the projected concentration field $\chi_1(t)$ (dashed line) and to that estimated from equation 14. a) permeability field variance $\sigma^2_{\ln K} = 0.01$, b) permeability field variance $\sigma^2_{\ln K} = 1$, c) permeability field variance $\sigma^2_{\ln K} = 9$.

A. Equivalence of $-\frac{1}{2}\frac{\partial}{\partial t}M(t)$ and $\int_\Omega d^d x D\nabla c(\mathbf{x},t)\cdot\nabla c(\mathbf{x},t)$

We start with the standard advection diffusion equation for conservative component c

$$\frac{\partial c(\mathbf{x},t)}{\partial t}+\nabla\cdot\Big(\mathbf{v}(\mathbf{x})c(\mathbf{x},t)\Big)=D\nabla^2 c(\mathbf{x},t) \tag{15}$$

Multiplying (15) by $c(\mathbf{x},t)$ and integrating over the spatial domain we obtain

$$\begin{aligned}&\frac{1}{2}\frac{\partial}{\partial t}\int_\Omega d^d x c^2(\mathbf{x},t)+\frac{1}{2}\int_\Omega d^d x\nabla\cdot\Big(\mathbf{v}(\mathbf{x})c^2(\mathbf{x},t)\Big)\\ &=\frac{1}{2}D\int_\Omega d^d x\nabla\cdot\nabla c^2(\mathbf{x},t)-\int_\Omega d^d x D\nabla c(\mathbf{x},t)\cdot\nabla c(\mathbf{x},t)\end{aligned} \tag{16}$$

Applying the divergence theorem, the second term on the left hand side and first term on the right hand side (those terms with the divergence $\nabla.$ operator) are zero since there is no mass flux on the domain boundaries after the injection time. Note that this is true for a pulse initial injection but not for a continuous injection condition. This leaves

$$\frac{1}{2}\frac{\partial}{\partial t}\int_\Omega d^d x c^2(\mathbf{x},t)=-\int_\Omega d^d x D\nabla c(\mathbf{x},t)\cdot\nabla c(\mathbf{x},t) \tag{17}$$

Recalling the definition of $M=\int_\Omega d^d x c^2(\mathbf{x},t)$ and $\chi=\int_\Omega d^d x D\nabla c(\mathbf{x},t)\cdot\nabla c(\mathbf{x},t)$ from (2) and (7) one obtains from equation (17) that

$$\chi(t)=-\frac{1}{2}\frac{\mathrm{d}M(t)}{\mathrm{d}t}. \tag{18}$$

B. Mean Error of the Scalar Dissipation Rate

In this appendix we determine the mean error associated with a finite number of particles when calculating the mean scalar dissipation rate.

The concentration as estimated from the particle trajectories obtained from a random walk particle tracking simulation using N particles can be written as

$$c_N(\mathbf{x},t) = \frac{1}{N}\sum_{n=1}^{N}\prod_{i=1}^{d}\delta_{\lfloor\frac{x_i}{\Delta x_i}\rfloor,\lfloor\frac{x_i^{(n)}(t)}{\Delta x_i}\rfloor}\,{\Delta x_i}^{-1}, \tag{19}$$

where δ_{ij} denotes the Kronecker-Delta; $\lfloor x\rfloor$ denotes the floor function defined as $\lfloor x\rfloor = \max\{n\in\mathbb{Z}|n\le x\}$, Δx_i is the size of the sampling bin in i-direction, $x_i^{(n)}(t)$ is the i-th coordinate of the particle trajectory $\mathbf{x}^{(n)}(t)$. The latter is defined by the Langevin equation

$$\frac{\mathrm{d}\mathbf{x}(t)}{\mathrm{d}t} = \mathbf{q}[\mathbf{x}(t)] + \sqrt{2D}\boldsymbol{\xi}(t), \tag{20}$$

where $\boldsymbol{\xi}(t)$ is a standard Gaussian noise. The concentration distribution $c(\mathbf{x},t)$ then is defined by

$$c(\mathbf{x},t) = \prod_{i=1}^{d}\left\langle\delta_{\lfloor\frac{x_i}{\Delta x_i}\rfloor,\lfloor\frac{x_i(t)}{\Delta x_i}\rfloor}\right\rangle{\Delta x_i}^{-1} \tag{21}$$

for suitably chosen bin-sizes Δx_i. The angular brackets denote the average over all noise realizations.

The concentration distribution $c(\mathbf{x},t)$ is given in terms of $c_N(\mathbf{x},t)$ as

$$c(\mathbf{x},t) = c_N(\mathbf{x},t) + \Delta c(\mathbf{x},t), \qquad \Delta c(\mathbf{x},t) = c(\mathbf{x},t) - c_N(\mathbf{x},t). \tag{22}$$

We define the mean square error of the numerical concentration as

$$\sigma_N^2(\mathbf{x},t) = \left\langle \left[\Delta c(\mathbf{x},t)\right]^2 \right\rangle . \tag{23}$$

Using (19), and (22), we obtain

$$\begin{aligned}\sigma_N^2(\mathbf{x},t) = c(\mathbf{x},t)^2 &+ \frac{1}{N^2}\sum_{n\neq n'}^{N}\prod_{i=1}^{d}\Delta x_i{}^{-2}\left\langle \delta_{\lfloor\frac{x_i}{\Delta x_i}\rfloor,\lfloor\frac{x_i^{(n)}(t)}{\Delta x_i}\rfloor}\right\rangle\left\langle \delta_{\lfloor\frac{x_i}{\Delta x_i}\rfloor,\lfloor\frac{x_i^{(n')}(t)}{\Delta x_i}\rfloor}\right\rangle \\ &+ \frac{1}{N^2}\sum_{n=1}^{N}\prod_{i=1}^{d}\Delta x_i{}^{-2}\left\langle \delta_{\lfloor\frac{x_i}{\Delta x_i}\rfloor,\lfloor\frac{x_i^{(n)}(t)}{\Delta x_i}\rfloor}\right\rangle \\ &- 2c(\mathbf{x},t)\frac{1}{N}\sum_{n=1}^{N}\prod_{i=1}^{d}\Delta x_i{}^{-1}\left\langle \delta_{\lfloor\frac{x_i}{\Delta x_i}\rfloor,\lfloor\frac{x_i^{(n)}(t)}{\Delta x_i}\rfloor}\right\rangle \end{aligned} \tag{24}$$

where we decomposed the double sum originating from $c_N(\mathbf{x},t)^2$ into a summation over $n \neq n'$ and one over $n = n'$. In the latter we use that $\delta_{ij}\delta_{ij} = \delta_{ij}$. Using the definition (21) of $c(\mathbf{x},t)$ yields

$$\sigma_N^2(\mathbf{x},t) = \frac{c(\mathbf{x},t)}{N\Delta V} - \frac{c(\mathbf{x},t)^2}{N}, \tag{25}$$

where $\Delta V = \prod_{i=1}^{d}\Delta x_i$ is the volume of the sampling bin. Thus, the mean error of

$$M_N(t) = \int_\Omega \mathrm{d}^d x c_N(\mathbf{x},t)^2 \tag{26}$$

is given by

$$\Delta M_N(t) = \langle M_N(t) - M(t)\rangle = \int_\Omega \mathrm{d}^d x \sigma_N^2(\mathbf{x},t) = \frac{1}{N\Delta V} - \frac{M(t)}{N}. \tag{27}$$

And the mean error of

$$\chi_N(t) = -1/2\frac{\mathrm{d}M_N(t)}{\mathrm{d}t} \tag{28}$$

is obtained from the time derivative of (27) as

$$\Delta\chi_N(t) = \langle\chi_N(t) - \chi(t)\rangle = \frac{\chi(t)}{2N} \tag{29}$$

Thus, the mean relative error when estimating the scalar dissipation rate using random walk particle tracking decrease with the inverse particle number as N^{-1}. We run simulations with varying amounts of particles and found close agreements with the analytical solution.

FIGURE 1

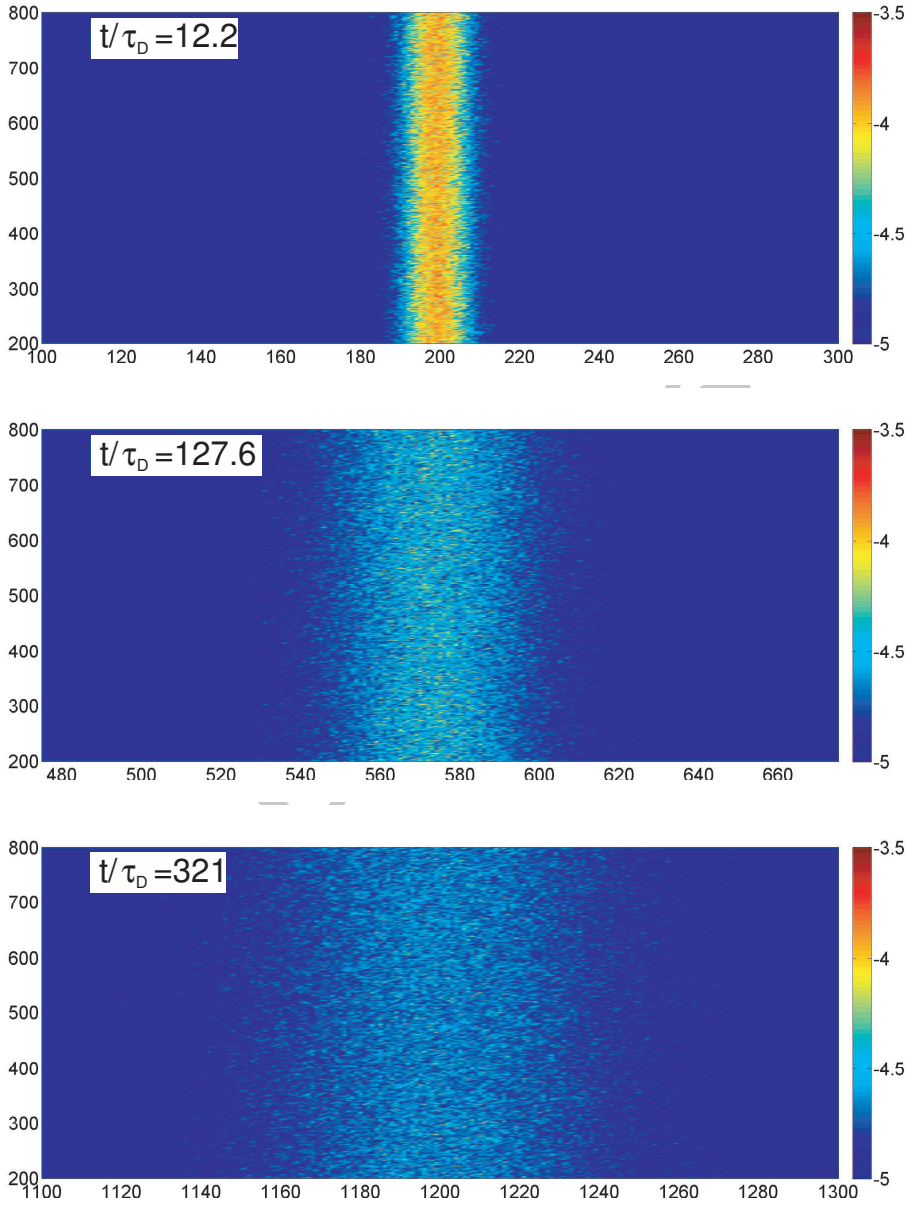

Figure 1. Spatial distribution of the concentration $c(x,t)$ simulated with 10^5 particles in a homogeneous porous medium at times a) $t/\tau_D = 12.2$, b) $t/\tau_D = 127.6$, c) $t/\tau_D = 321$. The color scale shows the logarithm of the concentration, computed with a bin size equal to the pixel size Δ_x.

FIGURE 2

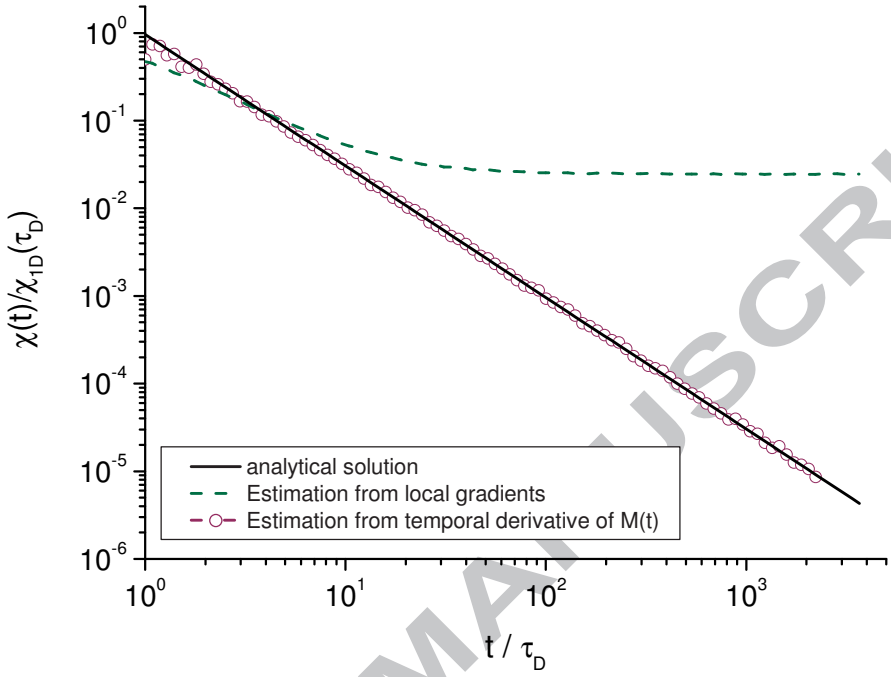

Figure 2. Time evolution of the scalar dissipation rate in a homogeneous medium, estimated from local concentration gradients and from the time derivative of $M(t)$. Notice the perfect overlap of the latter with the analytical solution.

FIGURE 3

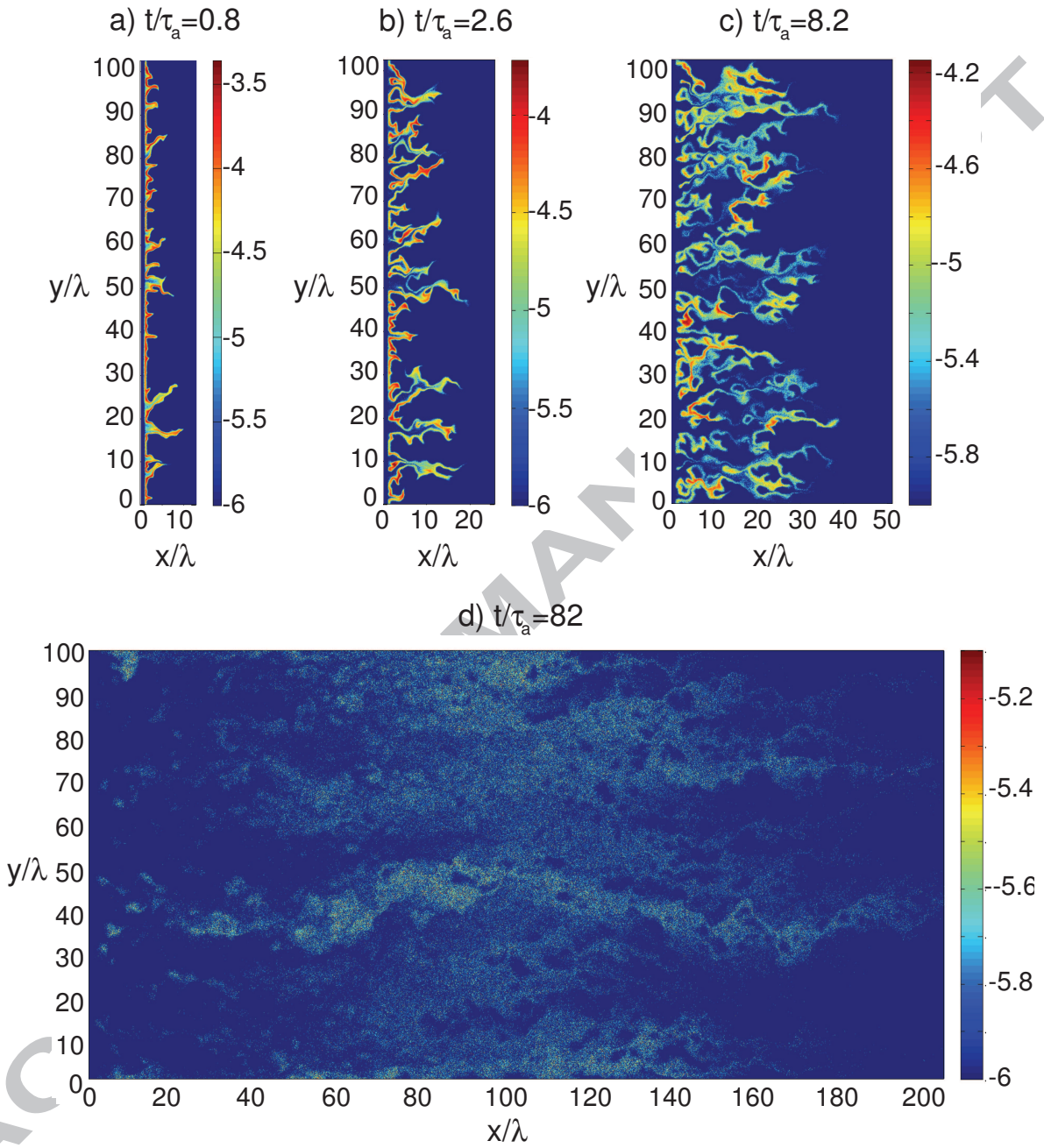

Figure 3. (color online). Spatial distribution of the conservative component $c(x,t)$ simulated for 10^6 particles in a highly heterogeneous porous medium at times a) $t/\tau_a = 0.8$, b) $t/\tau_a = 2.6$, c) $t/\tau_a = 8.2$, d) $t/\tau_a = 82$. The color scale shows the logarithm of the concentration, computed with a bin size equal to the pixel size Δ_x. The permeability field variance is $\sigma^2_{\ln K} = 9$, the correlation length $\lambda = 10$ and the Peclet number $Pe = 10^2$.

FIGURE 4

Figure 4. a) Characteristic spreading length (longitudinal standard deviation of the plume) and b) scalar dissipation rate estimated for permeability field variances ranging from $\sigma^2_{\ln K} = 0.01$ to $\sigma^2_{\ln K} = 9$ for a Peclet number $Pe = 10^2$.

a) spreading scale

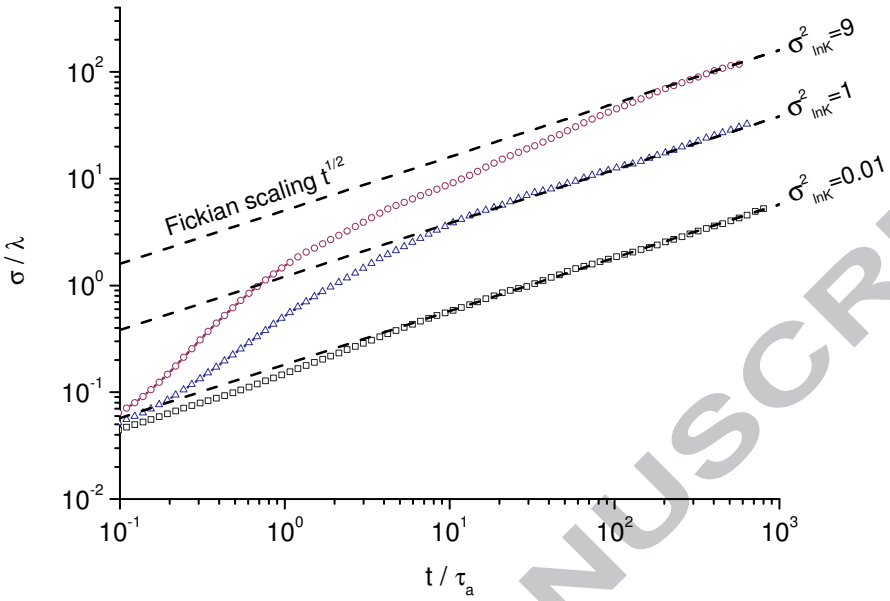

b) mixing rate

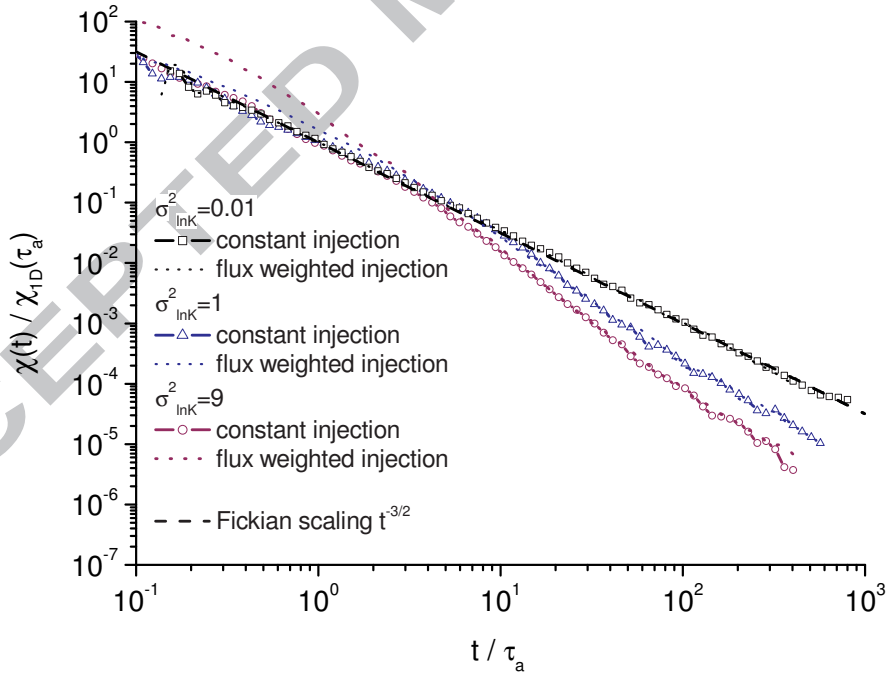

FIGURE 5

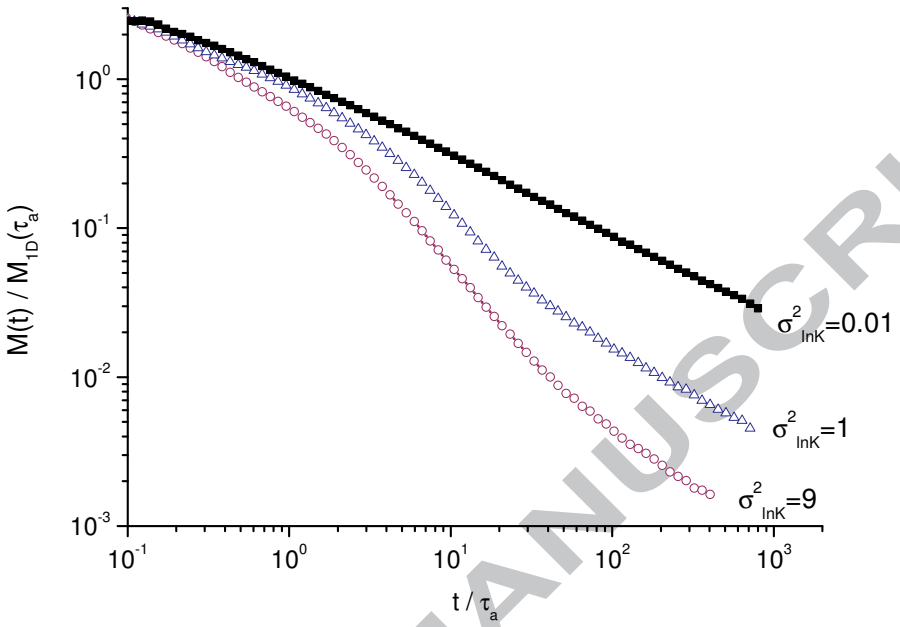

Figure 5. Time evolution of $M(t)$ for different permeability field variances. $M(t)$ is normalized by its expected value for the homogenenous domain at time $t = \tau_a$, $M_{1D}(\tau_a)$.

FIGURE 6

Figure 6. Scalar dissipation rate estimated from the full concentration field $\chi(t)$ (full line), compared to that estimated from the projected concentration field $\chi_x(t)$ (dashed line) and to that estimated from equation 14. a) permeability field variance $\sigma^2_{\ln K} = 0.01$, b) permeability field variance $\sigma^2_{\ln K} = 1$, c) permeability field variance $\sigma^2_{\ln K} = 9$.